Magnetic Resonance Imaging 85 (2022) 210–216

Contents lists available at ScienceDirect

Magnetic Resonance Imaging

journal homepage: www.elsevier.com/locate/mri

Technical Note

2D RF pulse design for optimized reduced field-of-view imaging at 1.5T and 3T

Orhun Caner Eren [a,b,c], Bahadir Alp Barlas [a,d], Emine Ulku Saritas [a,d,e,*]

[a] Department of Electrical and Electronics Engineering, Bilkent University, Ankara, Turkey
[b] Institute of Neuroinformatics, ETH Zurich, Zurich, Switzerland
[c] Department of Information Technology and Electrical Engineering, ETH Zurich, Zurich, Switzerland
[d] National Magnetic Resonance Research Center (UMRAM), Bilkent University, Ankara, Turkey
[e] Neuroscience Graduate Program, Bilkent University, Ankara, Turkey

ARTICLE INFO

Keywords:
Reduced field-of-view imaging
Two-dimensional RF pulse
Excitation profile
Off-resonance robustness
Diffusion weighted imaging

ABSTRACT

Two-dimensional spatially selective radiofrequency (2DRF) excitation pulses are widely used for reduced field-of-view (FOV) targeted high-resolution diffusion weighted imaging (DWI), especially for anatomically small regions such as the spinal cord and prostate. The reduction in FOV achieved by 2DRF pulses significantly improve the in-plane off-resonance artifacts in single-shot echo planar imaging (ss-EPI). However, long durations of 2DRF pulses create a sensitivity to through-plane off-resonance effects, especially at 3 T where the off-resonance field doubles with respect to 1.5 T. This work proposes a parameter-based optimization approach to design 2DRF pulses with blips along the slice-select axis, with the goal of maximizing slab sharpness while minimizing off-resonance effects on 1.5 T and 3 T MRI scanners, separately. Extensive Bloch simulations are performed to evaluate the off-resonance robustness of 2DRF pulses. Three different metrics are proposed to quantify the similarity between the actual and ideal 2D excitation profiles, based on the signals within and outside the targeted reduced-FOV region. In addition, simulations on a digital brain phantom are performed for visual comparison purposes. The results show that maintaining a sharp profile is the primary design requirement at 1.5 T, necessitating the usage of relatively high slab sharpness with a time-bandwidth product (TBW) around 8–10. In contrast, off-resonance robustness is the primary design requirement at 3 T, requiring the usage of a moderate slap sharpness with TBW around 5–7.

1. Introduction

Diffusion-weighted imaging (DWI) is becoming increasingly popular in the clinic due to its capability to probe white matter microstructure [1]. The most widely used technique during DWI data readout is single-shot echo-planar imaging (ss-EPI) due to its robustness against motion-induced phase issues in DWI, which can cause ghosting artifacts in multi-shot imaging sequences. However, since the entire *k*-space needs to be covered in one shot, ss-EPI images typically suffer from low resolution. Furthermore, ss-EPI images exhibit off-resonance-induced distortions due to long readout durations [2,3]. Reduced field-of-view (FOV) imaging methods have been proposed to alleviate these artifacts by decreasing the FOV along the phase encode (PE) direction and thereby enabling higher resolution images with fewer PE lines [4–9]. Several approaches such as two-dimensional (2D) spatially selective excitation [4,8], outer volume suppression [7] and zonal oblique multislice (ZOOM) echo-planar imaging (EPI) [10] show that reduced-FOV techniques can be applied successfully in various target regions. In particular, reduced-FOV techniques that utilize two-dimensional echo-planar radiofrequency (2DRF) pulses have found wide usage, especially in regions such as the spinal cord, breast, and prostate due to their fat-suppression capability while providing a sharp reduced-FOV profile along the PE-direction [11–14].

As aforementioned, the reduction in PE lines enhances the robustness against in-plane off-resonance artifacts for reduced-FOV ss-EPI. However, covering the excitation *k*-space in 2D requires long 2DRF pulses, increasing sensitivity to through-plane off-resonance effects, and causing a signal reduction in regions with large susceptibility variations [4]. Furthermore, these effects are bound to worsen at 3 T as the off-resonance field doubles with respect to 1.5 T. A potential solution to

* Corresponding author at: Electrical and Electronics Engineering, Bilkent University, Ankara, Turkey.
E-mail addresses: oreren@ethz.ch (O.C. Eren), barlas@ee.bilkent.edu.tr (B.A. Barlas), saritas@ee.bilkent.edu.tr (E.U. Saritas).

https://doi.org/10.1016/j.mri.2021.10.021
Received 15 July 2021; Received in revised form 15 October 2021; Accepted 16 October 2021
Available online 22 October 2021
0730-725X/© 2021 Elsevier Inc. All rights reserved.

overcome this problem is to incorporate the B_0 field map during the design of the 2DRF pulse [15]. While this technique achieves significant improvement against off-resonance effects, it requires acquiring an additional B_0 field map and computing subject-specific 2DRF pulses [15]. Therefore, there is a need to reduce through-plane off-resonance effects in 2DRF pulses that can be easily adopted in clinical settings.

One of the limitations of 2DRF based reduced-FOV imaging is that the 2D excitation generates replicas along the blipped direction (i.e., the discrete sampling axis in the excitation *k*-space). When the blipped direction is assigned as the slice-select (SS) axis, the replicas can cause a partial saturation effect in subsequent slice positions during multislice imaging [16,4,9]. This partial saturation may enforce a limit on the number of slices that can be imaged continuously without any signal loss. Overcoming this limitation necessitates longer 2DRF pulses, further exacerbating the aforementioned off-resonance sensitivity problem.

In this work, we propose a parameter-based optimization approach to alleviate off-resonance effects in 2DRF pulses with blips along the SS-axis. In this approach, the sharpness of the reduced-FOV profile in PE-direction and the maximum allowable slices for multislice imaging are chosen as free parameters, and the optimum values for these parameters are determined based on the signal levels in the targeted reduced-FOV region. Accordingly, three different metrics are proposed to quantify the similarity between the actual and ideal 2D excitation profiles, based on the signals within and outside the targeted reduced-FOV region. These metrics are then computed for off-resonance ranging up to 1 ppm to compare the off-resonance robustness of 2DRF pulses. Furthermore, the optimal parameters for 1.5 T and 3 T MRI scanners are compared via extensive simulations, including a visual comparison on a digital brain phantom. The results reveal the differences in the design requirements of 2DRF pulses for reduced-FOV imaging at 1.5 T and 3 T MRI scanners.

2. Theory and methods

2.1. 2D echo-planar RF pulse design

2DRF pulses allow the slice and slab profiles to be designed independently. The assignment of the axes as the "fast" and "slow" (i.e., blipped) directions is critical, since the replicas of the 2D excitation profile are generated along the blipped direction (see Fig. 1b). In this work, PE and SS axes were assigned as the fast and blipped directions, respectively (see Fig. 1a). This choice causes the fat profile to be shifted with respect to the water profile along the SS-direction, enabling fat suppression via a subsequent 180° RF pulse [4,9,16]. The 2DRF pulses are designed using the following equation:

$$B_1(t) = C(\alpha)A_{\mathrm{SS}}(k_{\mathrm{SS}}(t))A_{\mathrm{PE}}(k_{\mathrm{PE}}(t)) \parallel G(t) \parallel \tag{1}$$

Here, $k_{SS}(t)$ and $k_{PE}(t)$ are the SS and PE components of the excitation *k*-space trajectory, and A_{SS} and A_{PE} are designed based on the desired slice and slab profiles, respectively. Multiplication with $\|G(t)\|$, the norm of the gradient vector, adjusts the magnitude of the RF pulse in proportion with the trajectory speed. Lastly, $C(\alpha)$ tunes the overall amplitude of the RF pulse to achieve the desired flip angle, α. The slice and slab thicknesses, Δz and FOV_{slab}, can be expressed as follows:

$$\begin{aligned} \Delta z &= \frac{\mathrm{TBW_{SS}}}{K_{\mathrm{SS}}} \\ \mathrm{FOV_{slab}} &= \frac{\mathrm{TBW_{slab}}}{K_{\mathrm{slab}}} \end{aligned} \tag{2}$$

Here, TBW_{SS} and TBW_{slab} are the time-bandwidth products (TBW) indicating the slice and slab sharpnesses, respectively. In addition, K_{SS} and K_{slab} are the extents of the excitation *k*-space covered along the SS- and PE-directions, respectively. Note that FOV_{slab} corresponds to the reduced-FOV dimension along the PE-direction during imaging.

Since $k_{SS}(t)$ and $k_{PE}(t)$ follow an echo-planar trajectory in excitation *k*-space, the 2D excitation profile repeats along the blipped SS-direction. The distance between the replicas along the SS-direction, Δd_{SS}, can be expressed as follows:

$$\Delta d_{\mathrm{SS}} = \frac{N_{\mathrm{blip}}}{K_{\mathrm{SS}}} = \frac{N_{\mathrm{blip}}}{\mathrm{TBW_{SS}}}\Delta z \tag{3}$$

Here, N_{blip} is the number of blips along the SS-direction (i.e., the number of lines minus one for the 2DRF trajectory). In a multislice acquisition scheme, the replica excitations can cause a partial saturation effect, reducing the signal level for each slice [4,9]. The maximum number of slices, N_{max}, that can be imaged while avoiding this partial saturation effect can be expressed as the number of slices that can fit between two consecutive replicas, i.e.,

$$N_{\mathrm{max}} = \frac{\Delta d_{\mathrm{SS}}}{\Delta z} = \frac{N_{\mathrm{blip}}}{\mathrm{TBW_{SS}}} \tag{4}$$

Note that N_{max} can be increased by either increasing N_{blip} or decreasing TBW_{SS}, which in turn would cause either an increase in 2DRF pulse duration or a decrease in slice sharpness, respectively.

Due to chemical shift differences between fat and water molecules, the long duration of the 2DRF pulse causes a shift in the fat profile with

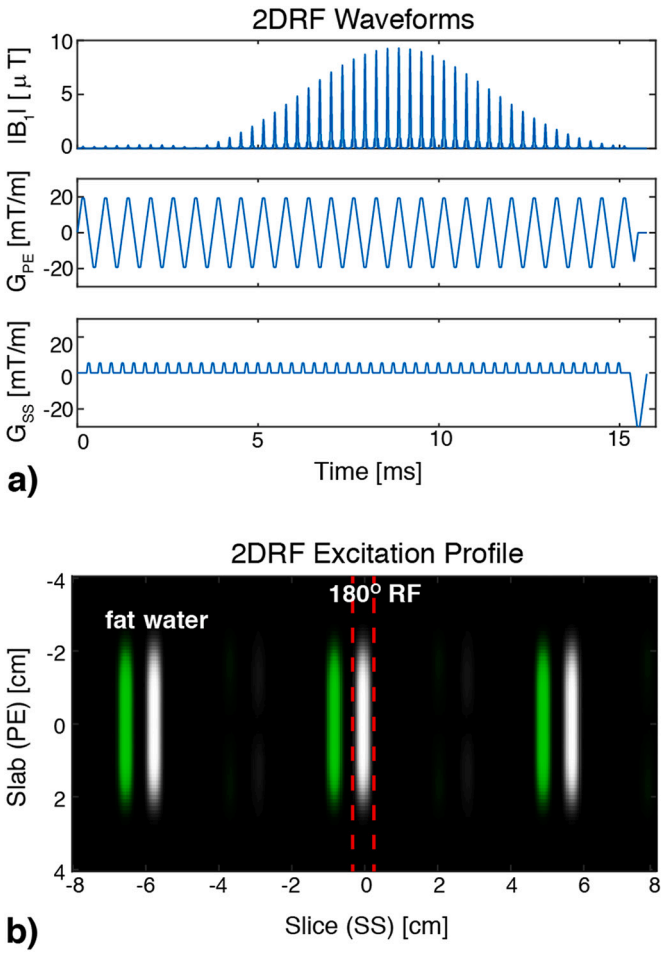

Fig. 1. An example 2DRF pulse, showing (a) RF and gradient waveforms, and (b) the corresponding 2D excitation profiles for water and fat, simulated for 440 Hz chemical shift at 3 T. The blipped nature of the gradient waveform in the SS-direction causes replicas to appear in the same direction, restricting the number of slices that can be imaged without experiencing partial saturation effects. Fat profile experiences a shift along the SS-direction proportional to the chemical shift in Hz. The parameters for this example 2DRF pulse were 15.3 ms pulse duration, $TBW_{slab} = 6$, $N_{max} = 16$, $FOV_{slab} = 4$ cm, $\Delta z = 4$ mm, and $TBW_{SS} = 3$.

respect to the water profile. This shift, Δd_{cs}, is along the blipped SS-direction and can be expressed as follows:

$$\Delta d_{cs} = \frac{N_{blip}}{K_{SS}} T_{fast} \Delta f_{cs} = \frac{N_{blip} T_{fast} \Delta f_{cs}}{TBW_{SS}} \Delta z \quad (5)$$

Here, K_{SS}/N_{blip} is the distance between the lines along the SS-direction of the 2DRF trajectory, T_{fast} is the duration per each line, and Δf_{cs} is the Larmor frequency difference between fat and water. As shown in Fig. 1b, typical 2DRF pulse durations result in 2D excitation profiles with no overlap between water and fat profiles, i.e., $\Delta d_{cs} \geq \Delta z$. The separation of the profiles allows a subsequent 180° refocusing pulse to select the water profile only, suppressing the signal from fat.

A direct consequence of Eq. (5) is that the 2DRF pulse is sensitive to off-resonance effects. Any source of B_0 field inhomogeneity (e.g., due to hardware imperfections or susceptibility differences) will cause an off-resonance frequency, Δf, which in turn will cause the excited slice to be shifted along the SS-direction. The amount of shift can be computed using Eq. (5), by replacing Δf_{cs} with Δf. Because the subsequent 180° refocusing pulse is considerably shorter in duration, its profile will not experience such a large shift, causing a mismatch between the excitation and refocusing profiles. In turn, this mismatch will cause the excited slice to be only partially refocused, resulting in a position-dependent signal loss in the corresponding reduced-FOV image [9]. To alleviate off-resonance sensitivity, the parameters of the 2DRF pulse need to be tuned carefully. During this tuning, multiple trade-offs emerge:

- While shorter T_{fast} reduces off-resonance sensitivity, it requires either FOV_{slab} to be enlarged or TBW_{slab} to be reduced. In return, larger FOV_{slab} worsens the in-plane off-resonance artifacts of the resulting ss-EPI image, whereas smaller TBW_{slab} sacrifices profile sharpness and causes a tapering of the signal along the PE-direction.
- While smaller N_{blip} reduces off-resonance sensitivity, it causes a reduction in N_{max}, hindering multi-slice acquisition performance.

In this work, we approach this problem from a brute-force parameter optimization perspective. We choose TBW_{slab} and N_{max} as the free parameters, which are then optimized separately for 1.5 T and 3 T cases to maximize off-resonance robustness.

2.2. 2DRF pulse parameters

All 2DRF pulses had $FOV_{slab} = 4$ cm, $\Delta z = 4$ mm, $TBW_{SS} = 3$. In the first part of the simulations, N_{max} was fixed at $N_{max} = 16$, and only TBW_{slab} was chosen as the free variable. Accordingly, 16 different 2DRF pulses were generated for TBW_{slab} ranging between 3 to 18. The resulting pulse durations ranged between 11.0 ms to 26.3 ms. An example 2DRF pulse with $TBW_{slab} = 6$ and 15.3 ms pulse duration is given in Fig. 1a, with the corresponding 2D excitation profile shown in Fig. 1b. Here, the fat profile was simulated assuming 440 Hz chemical shift at 3 T.

In the second part of the simulations, both N_{max} and TBW_{slab} were set as free variables. During this simulation, N_{max} was varied between 6 to 16 with steps of 2, and TBW_{slab} was varied between 3 to 18 while other parameters were kept fixed as given above. Accordingly, 96 different 2DRF pulses were generated and their performances were compared.

2.3. Simulations for off-resonance robustness

The off-resonance performances of 2DRF pulses were compared via Bloch simulations in MATLAB. Fig. 2a shows an "ideal" (but non-realistic) 2D excitation profile before applying 180° refocusing RF pulse. This ideal 2D excitation profile has value 1 within the targeted $\Delta z \times FOV_{slab}$ region and 0 outside. Fig. 2c shows the effective ideal 2D profile (referred to as "ideal 2D profile" from here on) after applying a realistic 180° RF pulse, where the effect of the 180° RF pulse can be seen

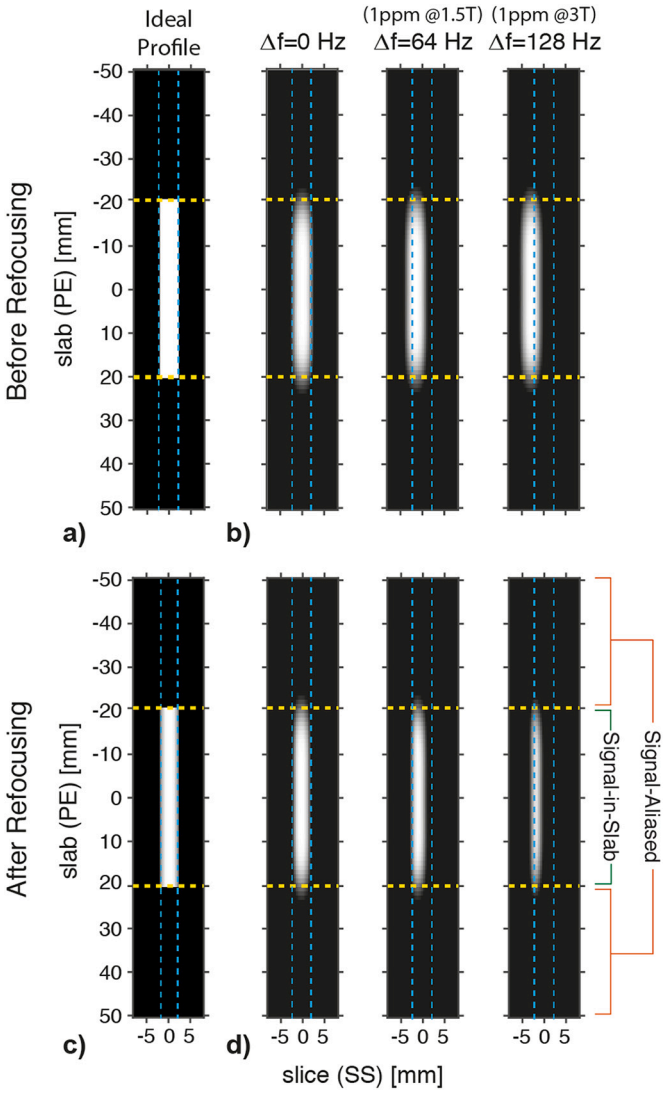

Fig. 2. Ideal 2D excitation profile and simulated 2D excitation profiles under off-resonance ranging up to 128 Hz. (a, c) Ideal 2D profiles before and after the 180° refocusing pulse, respectively. (b, d) Simulated 2D excitation profiles for the 2DRF pulse before and after the 180° refocusing pulse, respectively. The blue and yellow dashed lines mark the targeted Δz and FOV_{slab} positions, respectively. Due to duration/bandwidth mismatches between the 2DRF and 180° refocusing pulses, excitation profiles are only partially refocused, resulting in a thinner slice with increasing off-resonance. The portions of the 2D profile utilized for computing the metrics Signal-in-Slab and Signal-Aliased are marked, and ΔSignal is the difference between these two signals. The parameters for this example 2DRF pulse were 19.6 ms pulse duration, $TBW_{slab} = 10$, $N_{max} = 16$, $FOV_{slab} = 4$ cm, $\Delta z = 4$ mm, and $TBW_{SS} = 3$.

along the SS-direction. Based on this ideal 2D profile, three different metrics were defined to quantify the performance of a real 2D profile: Signal-in-Slab, Signal-Aliased, and ΔSignal. To compute these metrics, first the effective 2D profile after 180° RF pulse is computed for each 2DRF pulse, and this profile is integrated along the slice direction. Then, the resulting signal is integrated along the PE direction to compute the signals within and outside of the targeted FOV_{slab} portion. These values are then normalized by the integral of the signal within the targeted $\Delta z \times FOV_{slab}$ region for the ideal 2D profile, yielding Signal-in-Slab and Signal-Aliased as the normalized signals within and outside of the targeted reduced-FOV region, respectively. Here, the name Signal-Aliased refers to the fact that the excitation outside the targeted region along the PE direction (i.e., the undesired outer-volume excitation) ultimately

aliases back into the reduced-FOV image during imaging. Next, the difference between Signal-in-Slab and Signal-Aliased yields ΔSignal, a metric that rewards in-slab signal and penalizes aliased signal. Accordingly, for the ideal 2D profile, Signal-in-Slab is equal to 1, Signal-Aliased is equal to 0, and ΔSignal is equal to 1. Note that, even for a real 2DRF pulse, one can easily make Signal-in-Slab reach a value of 1 by arbitrarily extending the 2D excitation profile along the slab direction (e.g., by scaling down PE gradient amplitude), but doing so would cause excitation outside the targeted slab, causing an undesired increase in Signal-Aliased. Likewise, one can easily make Signal-Aliased go down to 0 by arbitrarily shrinking the 2D excitation profile along the slab direction, but this in turn would cause the Signal-in-Slab to fall down. In contrast, an arbitrary scaling of the 2D excitation profile would cause a decrease in ΔSignal. Thus, ΔSignal quantifies the similarity between a real 2D profile and the ideal 2D profile, with a value of 1 indicating a perfect match.

Here, we propose using ΔSignal to quantify the off-resonance robustness of a 2DRF pulse. In the absence of off-resonance effects, ΔSignal is expected to increase with increasing TBW_{slab} and TBW_{SS}, as the 2D excitation profile becomes sharper and approaches the ideal one. However, in the presence of off-resonance effects, the partial refocusing along the SS-direction will reduce ΔSignal at a level that strongly depends on the 2DRF pulse parameters. If a 2DRF pulse can maintain high ΔSignal levels in the presence of off-robustness, it can be said to be robust to off-resonance effects.

Next, for each 2DRF pulse, 2D excitation profiles were simulated with off-resonance ranging up to 1 ppm (i.e., up to 64 Hz for 1.5 T and up to 128 Hz for 3 T). A standard three-lobe sinc-shaped 180° RF pulse with 3.2 ms duration and 905 Hz bandwidth was utilized as the refocusing RF pulse. The 2D excitation profiles before and after the application of the 180° RF pulse were evaluated. The three metrics defined above were computed for each 2DRF pulse at each off-resonance value.

2.4. Simulations on brain phantom

To visually compare the 2DRF pulses, a digital T_2-weighted brain phantom was generated from a fuzzy brain model [17] after interpolating to a fine 3D grid of $0.5 \times 0.5 \times 0.25$ mm^3 voxel size. A realistic off-resonance field map was generated based on the anatomy of the phantom, causing 0.76±0.64 ppm (mean±std) off-resonance within the targeted reduced-FOV. The simulated 2D excitation profiles from different 2DRF pulses were applied on this brain phantom, mimicking a reduced-FOV T_2-weighted imaging scenario. The imaging parameters were $\Delta z = 4$ mm and FOV = 18×4 cm^2, where 4 cm corresponds to the reduced-FOV along the PE direction. Here, the effects of off-resonance during *k*-space data acquisition were ignored to better distinguish the non-idealities stemming from the 2DRF pulses alone.

3. Results and discussion

To visually demonstrate the effects of off-resonance, Fig. 2 shows ideal 2D profiles together with example 2D profiles for a 2DRF pulse with $TBW_{slab} = 10$, $N_{max} = 16$, and 19.6 ms pulse duration. Here, Fig. 2a demonstrates the ideal 2D excitation profile before 180° refocusing pulse, with value 1 within the targeted $\Delta z \times FOV_{slab}$ region and 0 outside. Likewise, Fig. 2c shows the ideal 2D profile after 180° refocusing pulse. Next, Fig. 2b shows the 2D excitation profiles before the 180° refocusing pulse, and Fig. 2d shows those after the 180° refocusing pulse for $\Delta f = 0$, 64 Hz, and 128 Hz cases. In each subfigure, the blue and yellow dashed lines mark the targeted Δz and FOV_{slab} positions, respectively. In Fig. 2b, the 2D excitation profiles demonstrates a large shift along the SS-direction, which is directly proportional to the off-resonance (see Eq. (5)). After the application of the 180° refocusing pulse, the shifted 2D excitation profiles are only partially refocused, resulting in a thinner slice, as seen in Fig. 2d for non-zero Δf cases. Comparing the results of $\Delta f = 64$ Hz and 128 Hz cases (i.e., 1 ppm off-resonance at 1.5 T and 3 T, respectively), one can deduce that 1 ppm off-resonance causes a significantly more pronounced signal loss at 3 T, as expected. The 2D profiles in Fig. 2d have Signal-in-Slab values of 0.83, 0.66, and 0.33, Signal-Aliased values of 0.027, 0.022, and 0.010, and ΔSignal values of 0.80, 0.64, and 0.32 for $\Delta f = 0$, 64 Hz, and 128 Hz, respectively.

To demonstrate the overall trends in the effects of off-resonance, Fig. 3 shows Signal-in-Slab, Signal-Aliased, and ΔSignal for the 2DRF pulse in Fig. 2 under off-resonance ranging up to 128 Hz. As seen in this figure, all three metrics decrease with off-resonance, as the mismatch between the 2D excitation and refocusing profiles grow with increasing off-resonance. For this sample 2DRF pulse, the mean values for Signal-in-Slab, Signal-Aliased, and ΔSignal across Δf ranging between 0 to 128 Hz are 0.63, 0.021, and 0.61, respectively.

Fig. 4 shows the results of the first part of the off-resonance robustness analysis, where N_{max} was fixed at 16 and only TBW_{slab} was set as the free variable. As shown in Fig. 4a, 2DRF pulse duration increases almost linearly with TBW_{slab}. The off-resonance robustness metrics (i.e., Signal-in-Slab, Signal-Aliased, and ΔSignal) were computed at off-resonance values of up to 1 ppm for 1.5 T and 3 T cases, separately. The mean values of these metrics within the 0–1 ppm range are plotted in Fig. 4b-d. Note that for the entire range of TBW_{slab} values, 2DRF pulses perform poorer in terms of off-resonance robustness performance at 3 T than at 1.5 T, as expected. As shown in Fig. 4b, while Signal-in-Slab is not significantly affected by TBW_{slab} at 1.5 T, it decreases rapidly with increasing TBW_{slab} at 3 T. Fig. 4c shows that the trends for Signal-Aliased are almost identical for 1.5 T and 3 T, decreasing with increasing TBW_{slab} due to sharper slab profiles achieved at higher TBW_{slab}. The similarity of the trends at 1.5 T and 3 T indicates that Signal-Aliased is only slightly altered by off-resonance and that it mainly depends on the tails of the slab profile, which are reduced with increasing TBW_{slab}. Fig. 4d shows that ΔSignal, considered as the main off-resonance robustness metric in this work, peaks at different TBW_{slab} values at 1.5 T and 3 T (marked with black in Fig. 4d). At 1.5 T, the optimum 2DRF pulse has $TBW_{slab} = 10$ with 19.6 ms duration. At 3 T, on the other hand, the optimum parameters are $TBW_{slab} = 6$ with 15.3 ms duration. It should be noted that 20 ms is the maximum allowed RF pulse duration in some MRI scanners, and hence the chosen optimum values remain within the practical duration limits. For the chosen range of parameters, all 2DRF pulses had fat suppression capability at both 1.5 T and 3 T, except for pulses with $TBW_{slab} < 5$ cases, which had this capability only at 3 T. Nonetheless, those pulses with small TBW_{slab} are far from ideal in terms of the slab sharpness that they provide.

In the second part of the off-resonance robustness analysis, both N_{max} and TBW_{slab} were set as free variables, and the other variables were kept the same as in the first part of the analysis. N_{max} was varied between 6 to 16 while TBW_{slab} was varied between 3 to 18. Fig. 5 shows the mean values of ΔSignal within the 0–1 ppm off-resonance range for the 1.5 T and 3 T cases. The results clearly demonstrate that ΔSignal peaks at

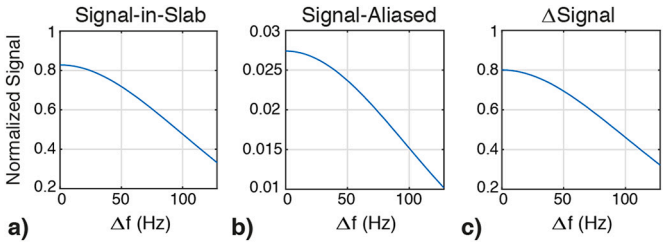

Fig. 3. Results of the off-resonance robustness simulation for the 2DRF pulse in under off-resonance ranging up to 128 Hz. (a) Signal-in-Slab, (b) Signal-Aliased, and (c) ΔSignal all decrease with off-resonance, with mean values of 0.63, 0.021, and 0.61, respectively, across Δf ranging between 0 to 128 Hz. The parameters for this example 2DRF pulse were 19.6 ms pulse duration, $TBW_{slab} = 10$, $N_{max} = 16$, $FOV_{slab} = 4$ cm, $\Delta z = 4$ mm, and $TBW_{SS} = 3$.

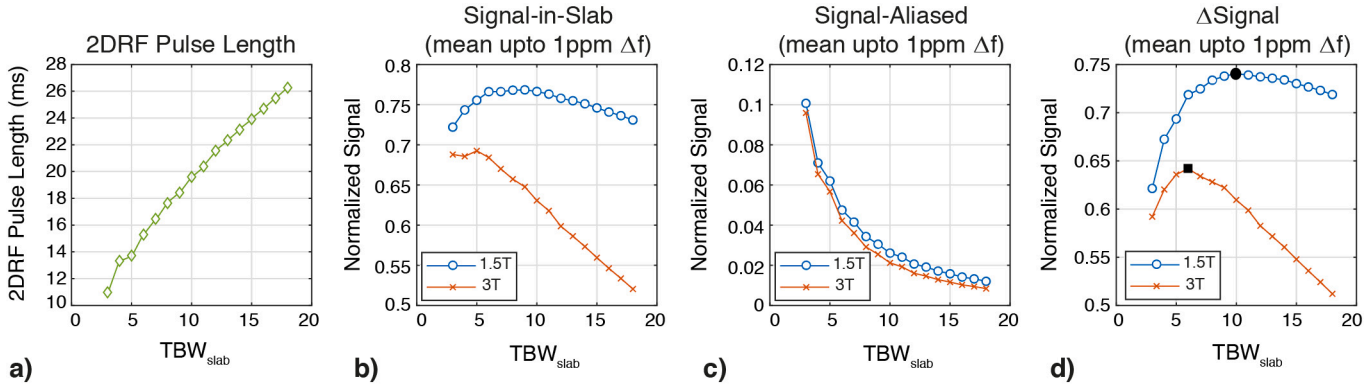

Fig. 4. Results of the first part of off-resonance robustness simulation, where N_{max} was fixed at 16 and only TBW_{slab} was set as the free variable. (a) 2DRF pulse duration increases almost linearly with TBW_{slab}. (b) Signal-in-Slab is only slightly affected by TBW_{slab} at 1.5 T, whereas it decreases rapidly with TBW_{slab} at 3 T. (c) The trends for Signal-Aliased are almost identical for 1.5 T and 3 T, decreasing with TBW_{slab}. (d) For 1.5 T, ΔSignal peaks for the 2DRF pulse with $TBW_{slab} = 10$ and 19.6 ms duration, while the best performing 2DRF pulse for 3 T has $TBW_{slab} = 6$ and 15.3 ms duration. Other parameters for the 2DRF pulses were $FOV_{slab} = 4$ cm, $\Delta z = 4$ mm, $TBW_{SS} = 3$.

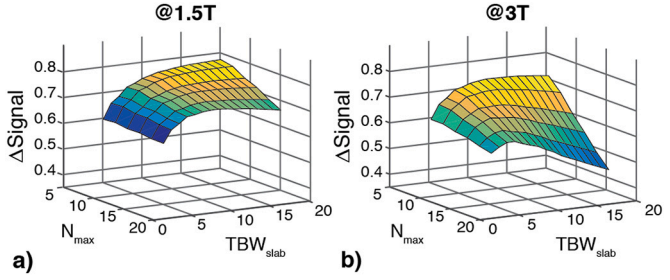

Fig. 5. Results of the second part of the off-resonance robustness analysis, where both N_{max} and TBW_{slab} were set as free variables. The mean values of ΔSignal at off-resonance ranging up to 1 ppm are shown for (a) 1.5 T and (b) 3 T. During these simulations, N_{max} was varied between 6 to 16 and TBW_{slab} was varied between 3 to 18. ΔSignal peaks at different combinations of N_{max} and TBW_{slab} values for 1.5 T and 3 T cases. The trends are mostly stable with respect to both N_{max} and TBW_{slab} for the 1.5 T case, whereas the 3 T case suffers from severe signal loss at higher values of N_{max} and TBW_{slab}. Other parameters for the 2DRF pulses were $FOV_{slab} = 4$ cm, $\Delta z = 4$ mm, $TBW_{SS} = 3$.

different combinations of N_{max} and TBW_{slab} values for the 1.5 T and 3 T cases. Accordingly, ΔSignal remains mostly stable with respect to both N_{max} and TBW_{slab} for the 1.5 T case. In contrast, higher N_{max} and TBW_{slab} reduce ΔSignal severely for the 3 T case due to the sensitivity of the 2DRF pulses to higher off-resonance effects at 3 T. Based on these results, we can deduce that one can utilize large N_{max} at 1.5 T with minimal sacrifice in signal, as long as TBW_{slab} is set to values around 8–10. Larger TBW_{slab} causes signal deterioration in the case of large N_{max}, and provides minimal improvement at small N_{max} at the cost of longer 2DRF pulses. In contrast, at 3 T, N_{max} needs to be kept as restricted as possible, and TBW_{slab} needs to be set to values around 5–7 to avoid excessive signal loss while providing sufficient slab sharpness.

In Fig. 6, the performances of the 2DRF pulses were compared visually via brain phantom simulations. For 1.5 T and 3 T, the optimum 2DRF pulses from the first part of the simulations were utilized (marked with black in Fig. 4d). The optimum pulses had $TBW_{slab} = 10$ (19.6 ms duration) and $TBW_{slab} = 6$ (15.3 ms duration) for the 1.5 T and 3 T cases, respectively. Fig. 6a shows the T_2-weighted brain phantom, with the targeted reduced-FOV region marked using red lines. Simulated off-resonance field maps at 1.5 T and 3 T were generated based on the anatomy of the phantom, and had 0.76±0.64 ppm (mean±std) off-resonance within the targeted reduced-FOV. Fig. 6b shows the slices after 2DRF excitation and 180° refocusing pulses for visual inspection. In addition, Fig. 6c shows the resulting reduced-FOV images with the FOV along the PE direction set to be the same as FOV_{slab} (i.e., 4 cm in this case). In these reduced-FOV images, aliasing occurs along the PE-direction if the slab profile is not sharp enough. Comparing the results in Fig. 6c, both 2DRF pulses perform similarly at 1.5 T in terms of signal level across the reduced-FOV images. However, the 2DRF pulse with $TBW_{slab} = 6$ causes prominent aliasing along the PE-direction (note the features marked with yellow arrows in Fig. 6a,c). This aliasing artifact, caused by insufficient slab sharpness, is considerably alleviated by the 2DRF pulse with $TBW_{slab} = 10$. For the 3 T results, the off-resonance induced signal loss becomes more significant in the corners of the reduced-FOV image for the 2DRF pulse with $TBW_{slab} = 10$, while the 2DRF pulse with $TBW_{slab} = 6$ provides sufficient signal level in the entirety of the image without inducing aliasing artifacts. Thus, the reduction of 2DRF pulse duration achieves an improvement of off-resonance robustness at 3 T without generating aliasing artifacts.

A potential approach to overcome the off-resonance sensitivity of the 2DRF excitation is to stretch the 180° RF pulse in time, so that its bandwidth matches that of the 2DRF pulse. Then, the refocusing and 2D excitation profiles would have identical slice shifts, producing a complete refocusing. However, the corresponding fat profiles would also have identical shifts, causing the fat suppression capability of the 2DRF/180° RF pulse pair to be lost entirely. Consequently, to avoid chemically-shifted fat artifact in ss-EPI, a separate fat suppression method such as spectral adiabatic inversion recovery would need to be incorporated [18]. With the fat suppressed, the acquired multi-slice volume would then reflect the water component warped along the SS-direction due to off-resonance induced slice shifts, which could be unwarped based on a B_0 field map. In contrast to this approach, the proposed parameter-based optimization technique does not require an additional fat suppression method, the acquisition of an additional B_0 field map, or unwarping of the multi-slice volume.

4. Conclusion

In this work, we demonstrate the need for different 2DRF pulse design specifications for reduced-FOV imaging at 1.5 T and 3 T MRI scanners to enhance off-resonance robustness and avoid aliasing. The proposed metrics, based on the signals within and outside the targeted reduced-FOV region, successfully quantify the off-resonance performance of 2DRF pulses. Extensive simulations for off-resonance robustness and imaging simulations on a digital brain phantom show that the primary requirement for the 2DRF pulse design at 3 T is off-resonance robustness. At 3 T, the maximum number of slices should be restricted and a moderate slab sharpness with a TBW of 5–7 should be utilized to avoid excessive signal loss. Conversely, profile sharpness in the PE-

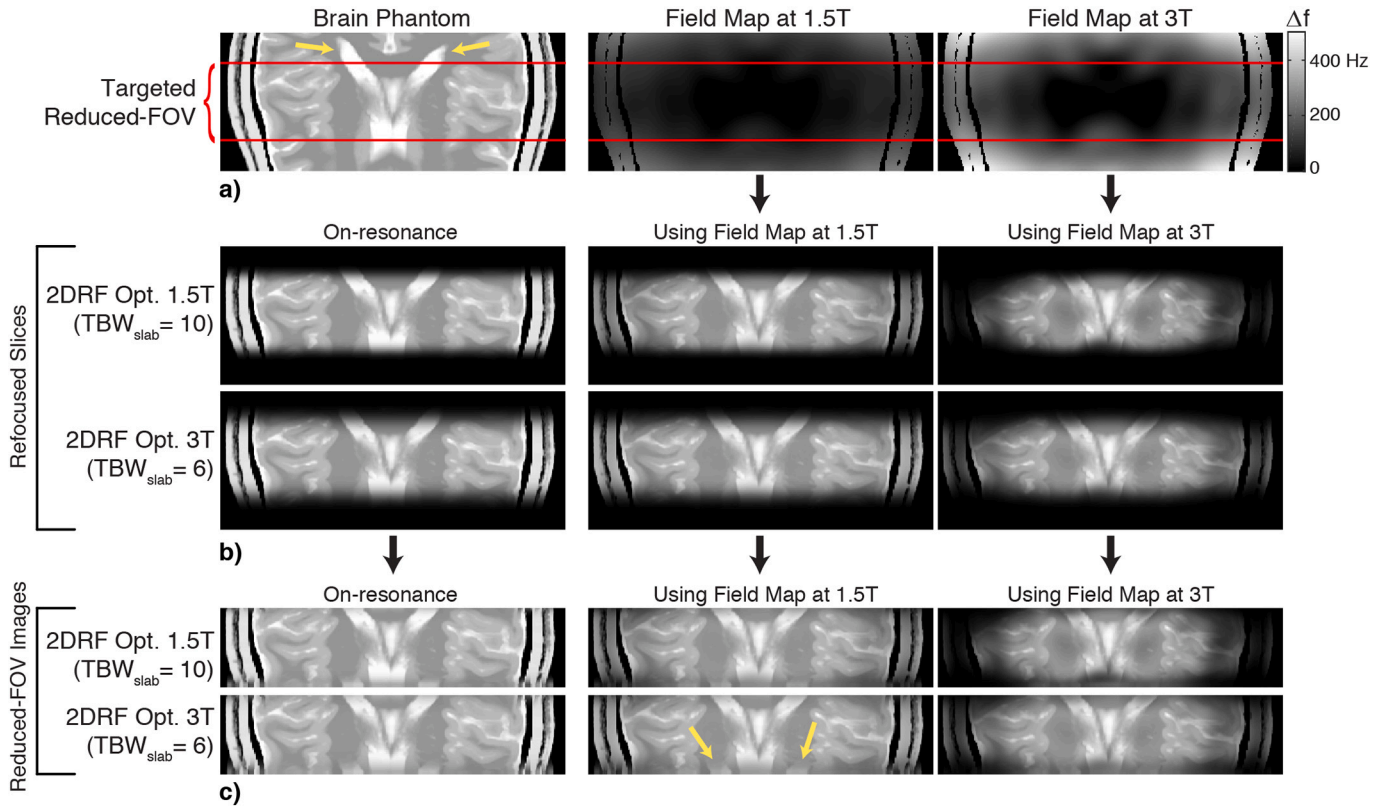

Fig. 6. Visual off-resonance robustness comparison on a digital brain phantom, for the optimum 2DRF pulses at 1.5 T and 3 T (marked with black in Fig. 4d). These pulses had $TBW_{slab} = 10$ (19.6 ms duration) and $TBW_{slab} = 6$ (15.3 ms duration) for the 1.5 T and 3 T cases, respectively. (a) The T_2-weighted brain phantom, and the field maps for 1.5 T and 3 T, which had 0.76±0.64 ppm (mean±std) off-resonance within the targeted reduced-FOV region (marked with red lines). (b) The slices after 2DRF excitation and 180° refocusing pulses and (c) the resulting reduced-FOV images with the FOV along the PE-direction set to be the same as FOV_{slab} (i.e., 4 cm in this case). The on-resonance images assume $\Delta f = 0$ throughout the volume. In 1.5 T simulations, the signal level is almost identical for both 2DRF pulses, but the aliasing along the PE-direction (marked with yellow arrows in both (a) and (c)) is more prominent in the image for the pulse with $TBW_{slab} = 6$. In 3 T simulations, the off-resonance induced signal loss is more significant in the corners of the image for the pulse with $TBW_{slab} = 10$, whereas the pulse with $TBW_{slab} = 6$ achieves an improvement in the signal level without generating aliasing artifacts.

direction is the primary design requirement at 1.5 T, allowing a large number of slices to be imaged as long as a relatively high slab sharpness with a TBW of 8–10 is utilized to avoid aliasing.

Acknowledgments

This work was supported by the Scientific and Technological Research Council of Turkey (TUBITAK) under Grant No: 117E116.

References

[1] Dietrich O, Biffar A, Baue-Melnyk A, Reiser MF. Technical aspects of:MR diffusion imaging of the body. Eur J Radiol 2010;76(3):314–22. https://doi.org/10.1016/j.ejrad.2010.02.018.
[2] Bihan DL, Mangin JF, Poupon C, Clark C, Pappata S, Molko N, Chabriat H. Diffusion tensor imaging: concepts and applications. J Magn Reson 2001;13(4):534–46. https://doi.org/10.1002/jmri.1076.
[3] Tournier JD, Mori S, Leemans A. Diffusion tensor imaging and beyond. Magn Reson Med 2011;65(6):1532–56. https://doi.org/10.1002/mrm.22924.
[4] Saritas EU, Cunningham CH, Lee JH, Han ET, Nishimura DG. DWI of the spinal cord with reduced:FOV single-shot:EPI. Magn Reson Med 2008;60(2):468–73. https://doi.org/10.1002/mrm.21640.
[5] Wheeler-Kingshott CAM, Hickman SJ, Parker GJM, Ciccarelli O, Symms MR, Miller DH, Barker GJ. Investigating cervical spinal cord structure using axial diffusion tensor imaging. NeuroImage 2002;16(1):93–102. https://doi.org/10.1006/nimg.2001.1022.
[6] Jeong E, Kim S, Guo J, Kholmovski EG, Parker DL. High-resolution:DTI with:2D interleaved multislice reduced:FOV single-shot diffusion-weighted:EPI (:2D ss-r:FOV-:DWEPI). Magn Reson Med 2005;54(6):1575–9. https://doi.org/10.1002/mrm.20711.
[7] Wilm BJ, Swensson J, Henning A, Pruessmann KP, Boesiger P, Kollias SS. Reduced field-of-view:MRI using outer volume suppression for spinal cord diffusion imaging. Magn Reson Med 2007;57(3):625–30. https://doi.org/10.1002/mrm.21167.
[8] Finsterbusch J. High-resolution diffusion tensor imaging with inner field-of-view:EPI. Magn Reson Med 2009;29(4):987–93. https://doi.org/10.1002/jmri.21717.
[9] Banerjee S, Nishimura DG, Shankaranarayanan A, Saritas EU. Reduced field-of-view:DWI with robust fat suppression and unrestricted slice coverage using tilted:2DRF excitation. Magn Reson Med 2016;76(6):1668–76. https://doi.org/10.1002/mrm.26405.
[10] Wheeler-Kingshott CAM, Parker GJM, Symms MR, Hickman SJ, Tofts PS, Miller DH, Barker GJ. :ADC mapping of the human optic nerve: increased resolution, coverage, and reliability with: Magn Reson Med 2002;47(1):24–31. https://doi.org/10.1002/mrm.10016.
[11] Andre JB, Zaharchuk G, Saritas EU, Komakula S, Shankaranarayan A, Banerjee S, Rosenberg J, Nishimura DG, Fischbein N. Clinical evaluation of reduced field-of-view diffusion-weighted imaging of the cervical and thoracic spine and spinal cord. AJNR Am J Neuroradiol 2012;33(10):1860–6. https://doi.org/10.3174/ajnr.A3134.
[12] Zaharchuk G, Saritas EU, Andre JB, Chin CT, Rosenberg J, Brosnan TJ, Shankaranarayan A, Nishimura DG, Fischbein NJ. Reduced field-of-view diffusion imaging of the human spinal cord: comparison with conventional single-shot echo-planar imaging. AJNR Am J Neuroradiol 2011;32(5):813–20. https://doi.org/10.3174/ajnr.A2418.
[13] Singer L, Wilmes LJ, Saritas EU, Shankaranarayan A, Proctor E, Wisner DJ, Chang B, Joe BNJ, Nishimura DG, Hylton NM. High-resolution diffusion-weighted magnetic resonance imaging in patients with locally advanced breast cancer. Acad Radiol 2012;19(5):526–34. https://doi.org/10.1016/j.acra.2011.11.003.
[14] Korn N, Kurhanewicz J, Banerjee S, Starobinets O, Saritas E, Noworolski S. Reduced-fov excitation decreases susceptibility artifact in diffusion-weighted MRI with endorectal coil for prostate cancer detection. Magn Reson Imaging 2015;33(1):56–62. https://doi.org/10.1016/j.mri.2014.08.040.
[15] Schneider R, Ritter D, Haueisen J, Pfeuffer J. :B0-informed variable density trajectory design for enhanced correction of off-resonance effects in parallel

transmission. Magn Reson Med 2014;71(4):1381–93. https://doi.org/10.1002/mrm.24780.
[16] Alley MT, Pauly JM, Sommer FG, Pelc NJ. Angiographic imaging with:2D RF pulses. Magn Reson Med 1997;37(2):260–7. https://doi.org/10.1002/mrm.1910370220.
[17] Cocosco CA, Kollokian V, Kwan RK-S, Pike GB, Evans AC, Brainweb:. Online interface to a:3D:MRI simulated brain database. NeuroImage 1997;5:425.
[18] Rosenfeld D, Panfil SL, Zur Y. Design of adiabatic pulses for fat-suppression using analytic solutions of the bloch equation. Magn. Reson. Med. 1997;37(5):793–801. https://doi.org/10.1002/mrm.1910370524.